Microstructure, and Physical and Mechanical Properties of Copper–Graphite Composites Obtained by In Situ Reaction Method

Zhu Xiao, Rushi Chen, Xuefeng Zhu, Zhou Li, Guofu Xu, Yanlin Jia, and Yunhe Zhang

The copper–graphite metal matrix composites were prepared by powder metallurgy method using cuprous oxide and graphite as the raw materials. Their microstructure, relative density, hardness, electrical resistivity and the compressive strength of the cuprous oxide–graphite (Cu₂O-Gr) composites were studied. This composite when compared with copper–graphite (Cu-Gr) composites using copper powder and graphite demonstrated that the new composite had finer microstructures with increased to the higher compression strength value. The Brinell hardness is about 1.5-1.6 times higher than the original material and the compressive strength increased by 50-100 MPa. The good parameters can be attributed to the redox reaction that occurs at the interface between cuprous oxide and graphite particles, resulting in uniform distribution of the reinforcements in matrix and strong interfacial bonding between the copper matrix and the graphite particles.

1. Introduction

The copper–graphite composite combines the high electrical conductivity, thermal conductivity, good plastic processing characteristics of copper and the self-lubricating performance, wear-resisting and corrosion resistance of graphite, resulting in its better comprehensive performance, and being promising in wide application fields (Ref 1, 2). However, the bonding between copper and graphite atoms is quite weak, resulting in the worse interface, coarse microstructure and large porosity in copper–graphite composite (Ref 3, 4). Bocchini (Ref 5) proved that the degree of porosity could have a strong negative effect on the levels of some functional characteristics. Especially, in order to obtain low friction, the content of graphite is often very high in copper–graphite composite, which further lowers the mechanical properties (i.e., hardness and fracture strength) of the composites (Ref 6, 7).

In recent years, many researches have been done to improve the interface strength between the copper and graphite. It was reported that the treatment of copper or nickel coating on graphite particles could improve the wettability between the copper matrix and graphite and increase the mechanical and tribological performances of copper–graphite composites (Ref 3, 6, 8). However, the coating process including the surface treatment and electroless plating was quite complicated, allied their high-cost and that do not favor the environment-friendly due to the use of a lot of chemical reagents (Ref 9).

Besides the interface strength, the size and the distribution of the solid lubricants can also strongly influence the mechanical performances of copper–graphite composites (Ref 10). Samal et al. (Ref 11) prepared fine composition powders by milling and found that the sintered copper–graphite composite using these milled powders had high density and hardness due to less porosity. Kováčik et al. (Ref 6) also found that the copper–graphite composite fabricated with 16-μm graphite particles had lower friction coefficient than that fabricated with 40-μm graphite particles, as the composites using fine graphite particles showed better spatial distribution of solid lubricants in the matrix. Beside, the good spatial distribution of graphite particles led to more continuous self-lubricant layer at the contact surface. Therefore, it is evident from the above research findings that the size reduction and the uniform distribution of graphite particles have major influence on the mechanical and tribological properties of copper–graphite composites. However, the smaller-sized uncoated graphite particles are easy to agglomerate due to high-order inter-particle force when using them directly to fabricate copper–graphite composites, which may result in the decrease in the mechanical properties of the copper–graphite composites (Ref 1, 6).

The addition of alloying elements such as Ti, Zr and Cr into copper could also improve the interface of a copper–graphite system because of the appearance of carbide (Ref 12-14). Considerable research efforts have also focused on finding novel lubricants that can potentially avoid/reduce negative effects on the properties of composites, e.g., electrical and thermal conductivity. It was reported that applying tungsten disulfide (WS₂) with the lamellar structure just like graphite (Ref 4, 15), MoS₂ (Ref 16), graphene nanosheets (Ref 17),

Zhu Xiao, Guofu Xu, and Yanlin Jia, School of Materials Science and Engineering, Central South University, Changsha 410083, China; and Key Laboratory of Non-ferrous Metal Materials Science and Engineering, Ministry of Education, Changsha 410083, China; Rushi Chen, Xuefeng Zhu, and Yunhe Zhang, School of Materials Science and Engineering, Central South University, Changsha 410083, China; and Zhou Li, School of Materials Science and Engineering, Central South University, Changsha 410083, China; and State Key Laboratory for Powder Metallurgy, Central South University, Changsha 410083, China. Contact e-mails: xiaozhumse@163.com, lizhou6931@163.com, and jiayanlin@126.com.

carbon nanotubes (Ref 18) or some other solid lubricants to replace graphite as the reinforcement in the copper phase could also improve the performances of Cu–solid lubricant composites. However, the effect of these methods mentioned above on the properties of the composite was still limited and with cost often high.

Nowadays, the metal material products are developing toward the direction of low-cost, efficient and environmental friendly process. Cuprous oxide (Cu_2O) is a typical oxidant of optimum chemical stability, and it could be reduced into copper by graphite only at high temperature. Applying cuprous oxide to replace copper to fabricate the copper–graphite composites could be a new effective method to improve the performances of copper–graphite composites. In this study, a novel 'in situ' reaction method was developed to fabricate the high-quality copper–graphite composite efficiently using cuprous oxide and graphite as the raw materials, and the microstructure and properties of this copper–graphite composite were investigated.

2. Experimental Procedure

2.1 Materials and Methods

The raw materials used in the experiment include cuprous oxide powder (supplied by the Aladdin Company Ltd, 99% purity, average particle size 5 μm, density: 6 g/cm³), spherical graphite powers (Gr, supplied by Qingdao Tengshengda Co., Ltd, 99.95% purity, average particle size 19 μm, density: 2.25 g/cm³) and electrolytic copper powder (supplied by Grinm Advanced Materials Co., Ltd, 99% purity, average particle size: 5 μm, density: 8.9 g/cm³). Figure 1 shows the morphology of cuprous oxide (a), electrolytic copper (b) and spherical graphite (c).

2.2 Mechanism of the 'In Situ' Reaction Method

In this experiment, the composites were produced using the hot pressing process. The difference between cuprous oxide–graphite (Cu_2O-Gr) composites and copper–graphite (Cu-Gr) composites is that there is a redox reaction occurred at the interface between cuprous oxide and graphite particles at a certain temperature.

The chemical reaction (1) would happen at first:

$$Cu_2O(s) + C(graphite) \rightarrow 2Cu(s) + CO(g) \uparrow \qquad (Eq\ 1)$$
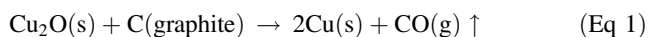
Because of the sufficient reducibility of CO, it is possible for the generated CO to continue reducing cuprous oxide just as shown in the following equation:

$$Cu_2O(s) + CO(g) \rightarrow 2Cu(s) + CO_2(g) \uparrow \qquad (Eq\ 2)$$
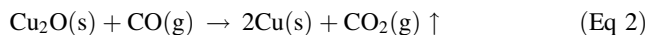
Therefore, the equation for the overall reaction might be:

$$2Cu_2O(s) + C(graphite) \rightarrow 4Cu(s) + CO_2(g) \uparrow \qquad (Eq\ 3)$$

These reactions happen at an atomic level, and it is expected that the in situ reaction would improve the bonding ability between the new generated copper and the residual graphite.

Table 1 gives the calculation results of thermodynamic parameters of the chemical reactions between Cu_2O and C or CO according to the thermodynamics formulas and data (Ref 19). According to the calculation results, it is found that the reaction (1) is always an endothermic reaction at both 20 and 850°C (the heat preservation temperature during the hot pressing process). The positive value of ΔrGm at 20°C means that the reaction (1) could not happen spontaneously; however, the molar reaction Gibbs energy turns to a negative value at 850°C so that it could occur at this temperature. This is attributed to the relatively higher temperature which can increase the trend of the endothermic reactions. Besides, the reaction (2) is always an exothermic and spontaneous reaction when the temperature is between 20 and 850°C. In addition, both the values of the molar formation Gibbs energy and the molar reaction Gibbs energy at 20 and 850°C for reaction (2) are close to each other, indicating that the temperature has little effect on reaction (2). Therefore, it could be concluded that the key condition for the redox reaction (3) is to trigger the reaction (1) which needs relatively higher activation temperature. And once the reaction (1) starts, it is easy for reaction (2) to happen.

The Cu_2O-Gr composites reinforced with 30, 40, 50 and 60 vol.% graphite (just expressed as Cu_2O-30Gr, Cu_2O-40Gr, Cu_2O-50Gr, Cu_2O-60Gr) were produced using cuprous oxide as the raw materials. For example, according to the final volume of graphite required, the Cu_2O-30Gr composite powder mixture should consist with 74 vol.% Cu_2O and 26 vol.% graphite before sintering. So that the final composition of the sintered composite would contain about 70 vol.% copper and 30 vol.% graphite, given that the cuprous oxide powders could be completely reduced by graphite during the hot pressing process according to reaction (3). The Cu-Gr composites using the mixture of pure copper and graphite powders were also
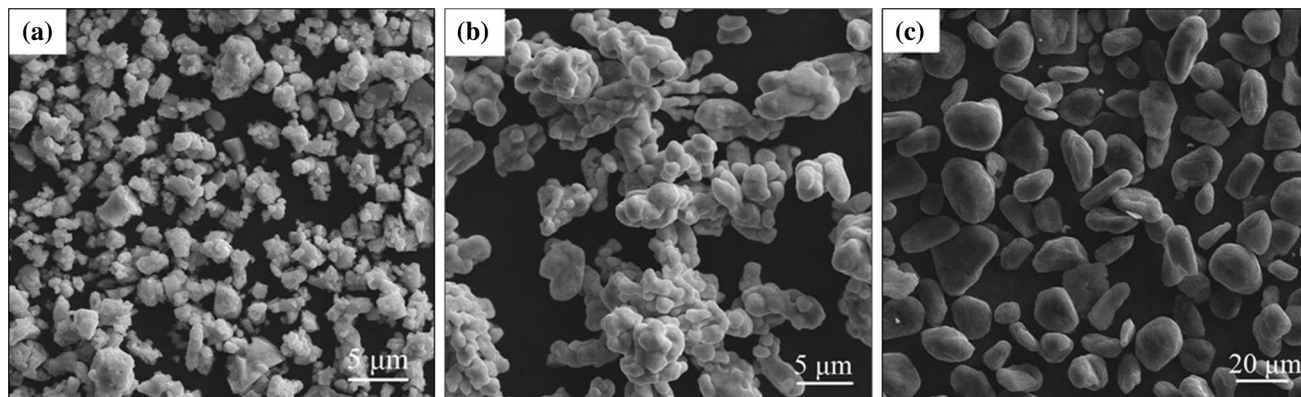

Fig. 1 SEM images of (a) cuprous oxide, (b) electrolytic copper powder and (c) spherical graphite

Table 1 Calculation results of thermodynamic parameters of the chemical reactions under the pressure of 0.01 Pa

Temperature, °C	Molar formation Gibbs energy $\Delta_f G_m$, KJ/mol			Molar reaction Gibbs energy $\Delta_r G_m$, KJ/mol		
	Cu_2O	CO	CO_2	Reaction (1)	Reaction (2)	Reaction (3)
25	− 146.0	− 287.7	− 544.8	− 141.7	− 111.2	− 252.8
850	− 103.8	− 337.8	− 546.3	− 234.0	− 104.7	− 338.8

Table 2 Compositions of the powder mixtures (before sintering) and the compacted composites (after sintering)

Composite	Powder mixture (before sintering)			Compacted composite (after sintering)	
	Cuprous oxide, vol.%	Copper, vol.%	Graphite, vol.%	Copper, vol.%	Graphite, vol.%
Cu_2O-30Gr	74	…	26	70	30
Cu-30Gr	…	70	30	70	30
Cu_2O-40Gr	67	…	33	60	40
Cu-40Gr	…	60	40	60	40
Cu_2O-50Gr	59	…	41	50	50
Cu-50Gr	…	50	50	50	50
Cu_2O-60Gr	51	…	49	40	60
Cu-60Gr	…	40	60	40	60

made for comparison. The detailed compositions of the composites are shown in Table 2.

2.3 Composites Preparation Process

In order to increase the roughness of the surface, graphite particles were first purified and oxidized by sonication in nitric acid for 45 min at 90-100°C and then dried in vacuum oven in 60°C for 5 h. The cuprous oxide powders and graphite powders were weighted in the pre-specified ratio (see Table 2) and mixed in a plastic beaker. A small amount of ethanol (approximately 2-3 vol.% of the mixture) was added to the mixture to act as a binding agent between the copper and graphite particles. The mixed powders were cold-pressed by a hydraulic machine at 200 MPa and then put into a copper pipe with a thickness of 0.8 mm.

The compacts were then hot-pressed in a vacuum of 10^{-2} Pa to form composites. The sintering process is shown in Fig. 2. During the sintering, Stage I could allow ethanol to evaporate, and then Stage II could help finishing the redox reaction adequately (the relatively lower pressure is to make a good contact between cuprous oxide and graphite powders and to remove the generated gas from the pores); lastly, Stage III was able to improve the sintering of the composites. For comparison, the compacts made by the mixture of copper and graphite powders were fabricated under the same conditions.

2.4 Characterizations, Mechanical and Electrical Properties

The sintered samples were cut and investigated for microstructual and mechanical properties. The microstructure of the sintered copper–graphite composites was analyzed by Leica EC3 optical microscopy (OM), Sirion 200 scanning electron microscopy (SEM) and DMAX-2500 x-ray diffraction analyzer, respectively. The density of the composites was measured according to Archimedes principle, and the Brinell hardness of the composites was measured by NEXUS Brinell
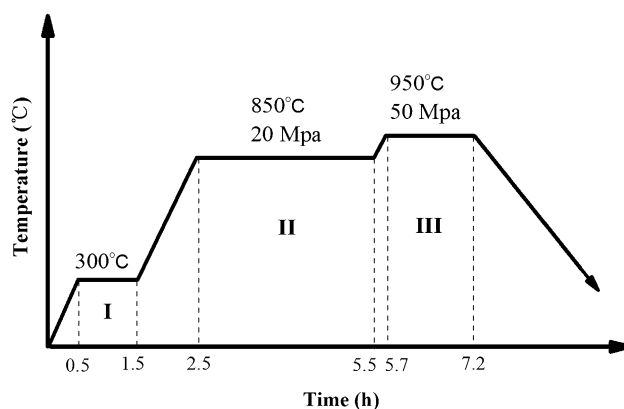
Fig. 2 Schematic diagram of the hot pressing process

hardness tester (3300-Model), with a test force of 62.5 kgf. Three specimens with dimensions of 5 mm × 5 mm × 5 mm were cut from different samples for density test, and the average value was taken. The Brinell hardness of each specimen was measured five times, and the average value of hardness was taken. The four probe method was used to measure the electrical resistance of the samples, and the SDY-4 D type four probe electrical conductivity tester was used. Three specimens with dimensions of 20 mm × 2 mm × 5 mm were cut from different samples for electrical test, and the average value was taken. Three compression test specimens with dimensions of 5 mm × 5 mm × 5 mm were used to obtain the compression strength of different sample, and the compression strength was evaluated by an Instron universal testing machine (3369-Model) with a crosshead speed of 2 mm/min. The friction property of the composites was tested on CSM Spin-on-disk tribometer under the normal laboratory atmosphere (50% relative humidity and 25°C), with the sliding speed of and normal load between 1 and 5 N. The disk was made by Cu-

0.4 Mg alloy. The dimension of the specimen is 3 mm × 3 mm × 8 mm, and the curvature radius at the contact end of the pin is 7 mm to maintain good contact between the pin and disk during sliding. The wear mass loss was calculated from the difference in the mass weighted by a digital microbalance (0.1 mg precision, model TE214S). The wear rate of the composites was calculated according to Ref 18. Three specimens were tested for each composite, and the average values of friction coefficient and wear loss were taken.

3. Result and Discussion

3.1 Mass Loss Calculation during the Reaction

In order to make sure the actual reactions during the sintering process, 150 g composite powder mixtures of Cu_2O-30Gr, Cu_2O-40Gr, Cu_2O-50Gr and Cu_2O-60Gr were heated in vacuum furnace at 850°C for 3.5 h with a vacuum of 10^{-2} Pa. Each sample was weighted before and after heating by a digital microbalance (0.1 mg precision) to calculate the real mass loss. The theoretical mass loss (*a*) was calculated according to the reaction (3), while the theoretical mass loss (*b*) was obtained if only reaction (1) succeed. The mass loss of composite powder mixtures with varying volume fraction of graphite powders is shown in Fig. 3. As observed in this figure, it is demonstrated that the line of real mass loss is very closer to the line of theoretical mass loss (*a*), suggesting the occurrence of both reaction (1) and reaction (2). So, although the graphite content in this investigation is more than 11.6 wt.% for all the range, the final products of the chemical reaction between Cu_2O and graphite are just Cu and CO_2.

3.2 Structure of Copper–Graphite Composite Fabricated by the 'In Situ' Reaction Method

3.2.1 XRD Analysis of the Composites. Figure 4 shows the XRD patterns of the Cu_2O-Gr composites and Cu-Gr composites with 30 vol.% and 50 vol.% graphite, respectively. The patterns of Cu_2O-Gr composites and Cu-Gr composites at any given graphite content are very similar to each other. It should be noted that only Cu peaks and C peaks are found in the patterns, and little residual Cu_2O is found in the Cu_2O-Gr composites, suggesting that nearly all the original cuprous oxide has been reduced to pure copper by graphite.

3.2.2 Microstructural Characterization. Figure 5(a) to (f) shows the typical OM images of Cu-Gr and Cu_2O-Gr composites, respectively, where the bright area corresponds of the copper, and the dark area for the graphite. It can be seen that the graphite particles distributed uniformly in the matrix of Cu-30Gr (Fig. 5a), but some of the graphites are agglomerated in Cu-50Gr (Fig. 5b). Compared with Cu-Gr composites, the graphite particles in Cu_2O-Gr composites have much smaller size and they are more homogeneously distributed in the copper matrix (Fig. 5c and d). It is attributed to the redox reaction between Cu_2O and graphite that occurs at the interface during the sintering process, which decreases the size of the graphite particles.

Figure 6(a) to (h) shows the SEM images of the prepared Cu-Gr and Cu_2O-Gr composites, respectively. The graphites in Cu-Cr composites still keep its original shape and size and are easy to pull out during polishing due to the weak interface bonding between the copper and the graphite (see Fig. 6a, b, c, and d). There are a lot of pores at the interface between the copper and the graphite or between the graphite particles (marked with circles in Fig. 6a, b, and c). The increase in volume fraction of graphite from 30% to 60% also leads to severe agglomeration of graphite particles. The SEM image of Cu-60Gr (see Fig. 6d) reveals the agglomerated graphite particles due to high-order inter-particle force. However, the shape and size of the graphite particle in Cu_2O-Gr composites are quite different from the original particles, and the shape of graphite changes from irregular or spherical shape to worm-like shape due to the redox reaction during sintering process, especially in Cu_2O-30Gr with a high content of Cu_2O. The average thickness of worm-like shape graphite particle in different Cu_2O-Gr composites was only about 3-5 μm. Few cracks and pores are found in the Cu_2O-Gr composites, even in the Cu_2O-60Gr specimen. Besides, the Cu_2O-Gr composites with 30 vol.%, 40 vol.% and 50 vol.% in Fig. 6(e), (f), and (g) show a much more homogeneous distribution of graphite in copper matrix than Cu-Gr composites. Even in Cu_2O-60Gr,
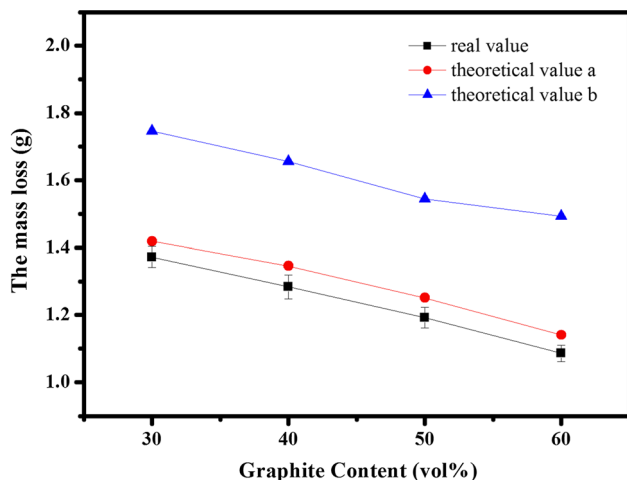
Fig. 3 Mass loss of composite powder mixtures with different volume fractions of graphite powders
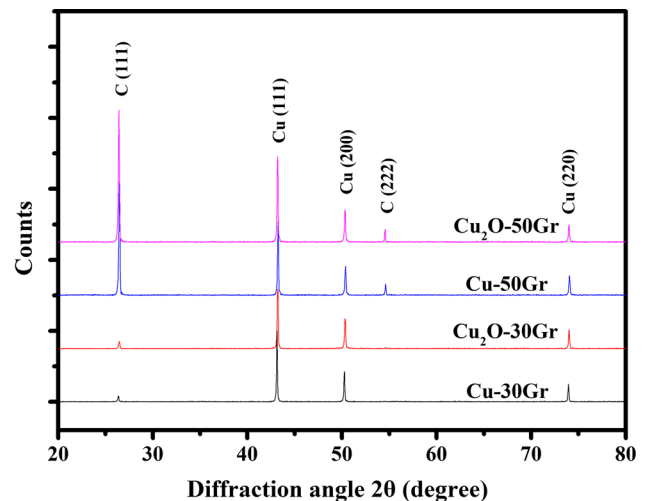
Fig. 4 XRD patterns of Cu_2O-Gr composites and Cu-Gr composites
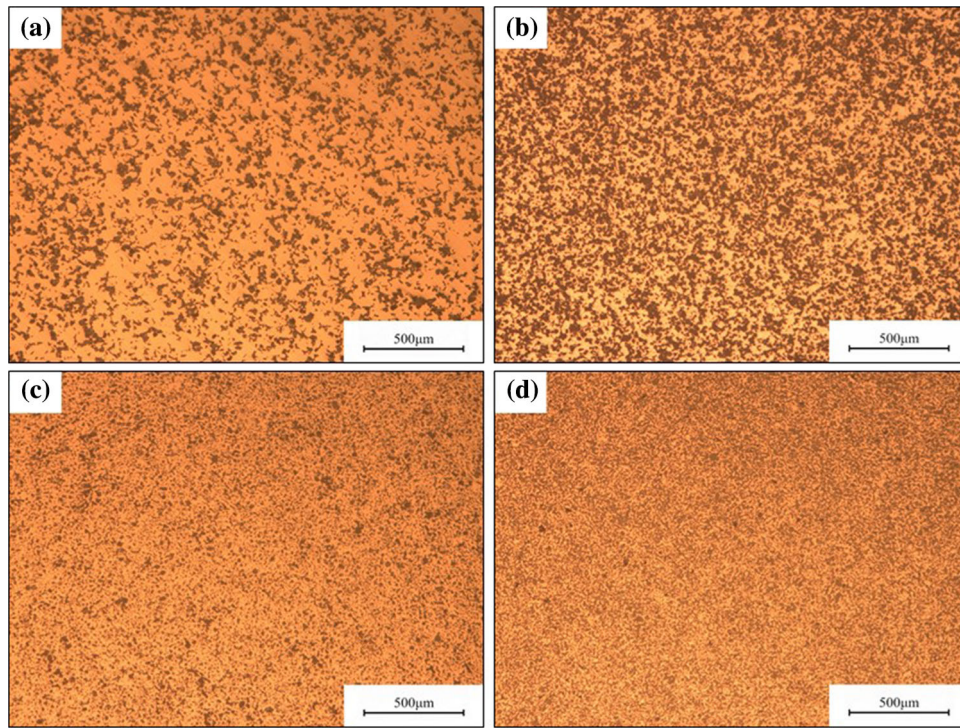
Fig. 5 OM images of Cu-Gr and Cu₂O-Gr composites: (a) Cu-30Gr, (b) Cu-50Gr, (c) Cu₂O-30Gr and (d) Cu₂O-50Gr

there are just a little agglomerates of graphite particles in the copper matrix. These indicate that the in situ reaction plays a significant role in changing the structure of copper–graphite composites.

In order to investigate the structure of interface between the copper matrix and the graphite, the microstructure of the composite was observed in high magnification. Figure 7 shows the SEM images of Cu-Gr and Cu₂O-Gr composites in high magnification. It can be seen that the bonding state between copper and graphite particles in Cu-Gr composite is relative poor, and some graphite particles are broken during sintering process. However, the interface between copper and graphite particle in Cu₂O-Gr composite is very clear and intact, suggesting that the graphite particles bond with the copper matrix well. This good interfacial integration should be attributed to the redox reaction between copper and graphite.

3.3 Properties of Copper–Graphite Composite Fabricated by the 'In Situ' Reaction Method

3.3.1 Density, Hardness of the Composites. Figure 8 shows the variations in relative density and Brinell hardness of Cu-Gr and Cu₂O-Gr composites with the graphite content. The relative density of the Cu₂O-Gr composite changes slightly with the graphite content, with a value of about 99.5-99.7%, while that of the Cu-Gr composites decreases with the increasing graphite content gradually. It is attributed to the poor wettability between the constituting elements and the aggregation of some graphite particles. With the increase in volume fraction of graphite particles, the cracks, fissures and pores would also be greatly increased. It should be noted that

the relative density of the Cu₂O-Gr composite is always higher than that of the Cu-Gr composite at any given graphite content. The higher relative density of Cu₂O-Gr composite should be attributed to the improved bonding between Cu and graphite in Cu₂O-Gr composites since the in situ reaction is processed by introducing Cu₂O as the raw materials. These results reinforced with the observed for the microstructures of the composites (SEM images). The increase in volume percentage of graphite in copper matrix leads to reduction in the hardness of composites due to the effect of the soft graphite. Besides, the increased tendency of crack initiation and propagation at the graphite–metal interface are also responsible for the decrease of hardness, and this variation of hardness are coherence with values obtained by other similar studies (Ref 20, 21).

The hardness of Cu₂O-Gr composites is 20-30 HB higher than that of Cu-Gr composites at any given graphite content. The maximum Brinell hardness value of around 37 HB is achieved for Cu-30Gr composite, whereas higher hardness value of around 56 HB is obtained for Cu₂O-30Gr composite. This demonstrates that the use of the cuprous oxide can significantly improve the mechanical properties of the composites.

3.3.2 Electrical Resistivity Parameter. Table 3 lists the electrical resistivity values for all Cu₂O-Gr and Cu-Gr composites containing different graphite contents. The electrical resistivity values increase with the graphite content gradually. It has been reported that the hindrance in the continuous network strongly influences the electrical conductivity of a metal matrix composite (MMC), and when volume percentage of graphite increases, the possibility of hindrance also increased, leading to the increase in electrical resistivity (Ref 21). It is interesting that the electrical resistivities of Cu₂O-Gr composite and Cu-Gr
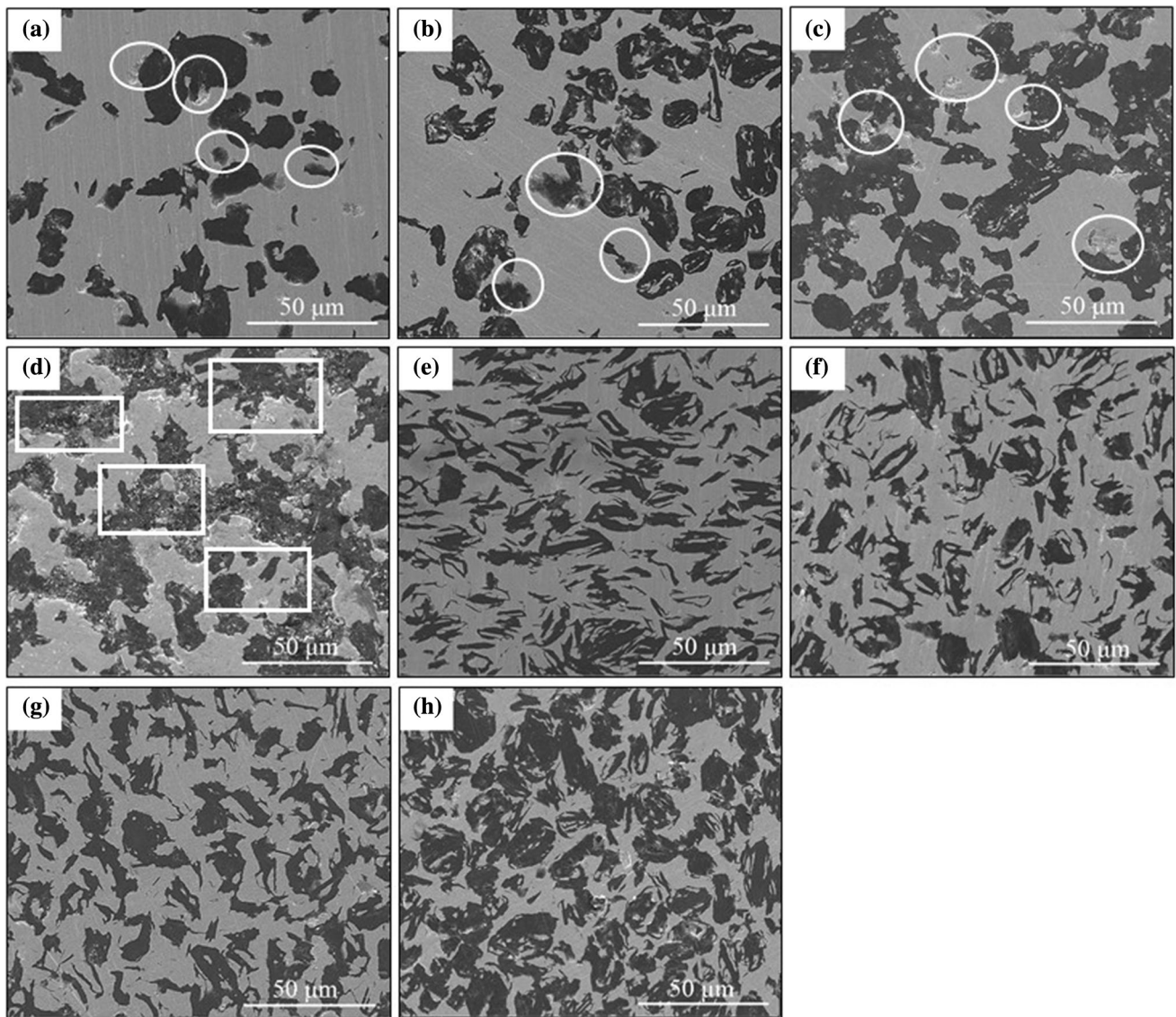
Fig. 6 SEM images of the composites: (a) Cu-30Gr, (b) Cu-40Gr, (c) Cu-50Gr, (d) Cu-60Gr, (e) Cu_2O-30Gr, (f) Cu_2O-40Gr, (g) Cu_2O-50Gr and (h) Cu_2O-60Gr

composite are close to each other, even if the interface bonding of Cu_2O-Gr composite is much strong, suggesting that the in situ reaction has little effect on the improvement in electrical conductivity.

Electrical energy in solids is conducted by two mechanisms: lattice vibration and migration of free electrons. The sum of these two contributions represents the total electrical conductivity of the solid medium (Ref 22). In metals, there are a lot of free electrons which can conduct electrical energy efficiently. The contribution of lattice waves to electrical energy conduction in metals can be ignored, and the conduction of electrical energy mainly results from the migration of free electrons. Thus, metals have a lower electrical resistivity than fluids and nonmetallic solids. In this experiment, the copper and the graphite have electrical resistivity of 0.01724 and 11 $\mu\Omega$ m, repetitively.

For the electrical resistivity of two phase materials, i.e., binary mixtures, three basic models have been established to predict the effective conductivity of mixtures: one for parallel arrangements, one for series arrangements and one for random continuous arrangements (Ref 23). The equations of the models are as follows (Ref 24):

$$\text{Parallel model}: \quad \lambda = V_1\lambda_1 + V_2\lambda_2 \tag{Eq 4}$$

$$\text{Series model}: \quad \lambda = \frac{1}{V_1/\lambda_1 + V_2/\lambda_2} \tag{Eq 5}$$

Continuous model (EMT model) :

$$V_1\frac{\lambda_1 - \lambda}{\lambda_1 + 2\lambda} + V_2\frac{\lambda_2 - \lambda}{\lambda_2 + 2\lambda} = 0 \tag{Eq 6}$$

where λ is the effective electrical resistivity of the mixture, λ_1 and λ_2 are electrical resistivity of the two phases and V_1 and V_2 are volume fractions of the two phases, respectively.

The above equations could be much accurate to solve the electrical problem when the two phases have similar electrical resistivity. However, the large difference of electrical resistivity and the electrical resistivity of the interface between the copper matrix and graphite may affect the electrical properties of the
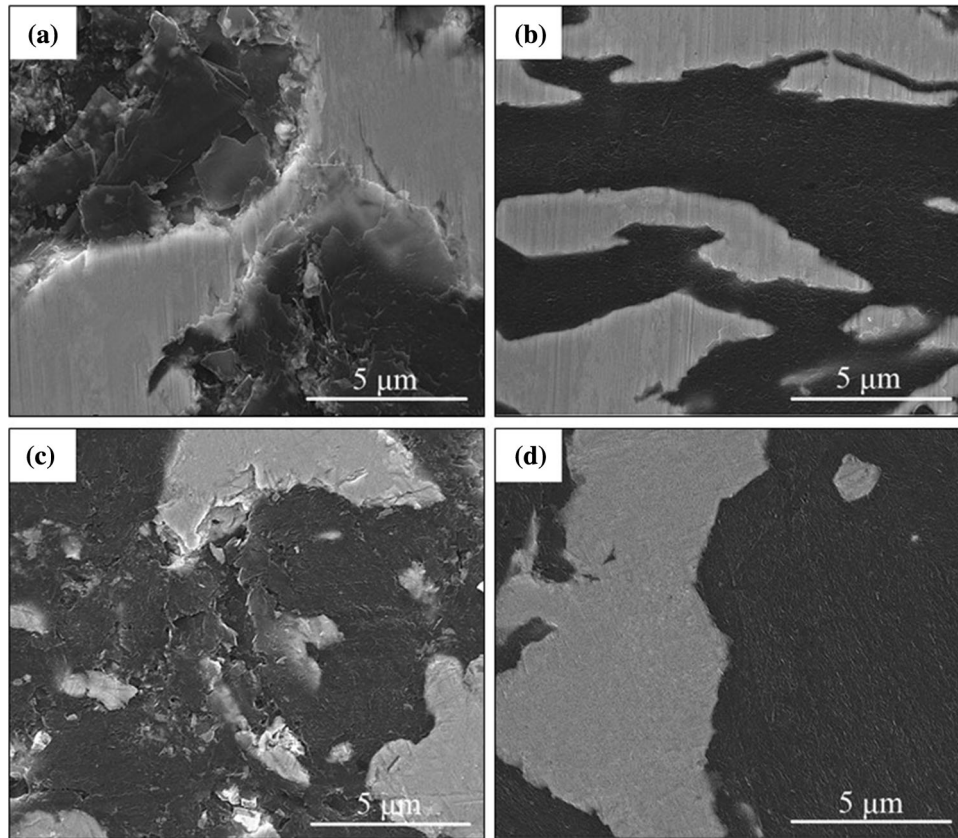
Fig. 7 SEM images of the composites in high magnification: (a) Cu-30Gr, (b) Cu$_2$O-30Gr, (c) Cu-50Gr and (d) Cu$_2$O-50Gr
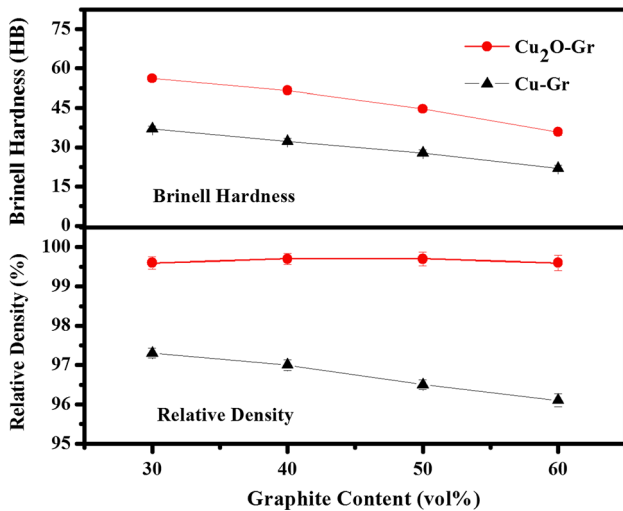

Fig. 8 Variations in relative densities and Brinell hardness of Cu-Gr and Cu$_2$O-Gr composites with the graphite contents

composite. A percolation theory based (PB) on the empirical correlation of the porous metal with the second phase of air has shown that the relationship between the electrical resistivity (λ/λ_c) and the volume fraction of the metal can be expressed by the power law (Ref 24):

$$\frac{\lambda}{\lambda_c} = V_c^n \qquad \text{(Eq 7)}$$

where λ is the electrical resistivity of the composite, λ_c is the electrical resistivity of the copper (0.01724 $\mu\Omega$ m), V_c is the volume fraction of copper and n is the exponent for electrical resistivity.

Figure 9 presents a comparison of the variation in relative electrical conductivity using parallel model, series model, EMT model and percolation model between Cu$_2$O-Gr composites and Cu-Gr composites with variation in graphite contents. The electrical conductivity of the composite increases with the increase of the content of copper. It is obvious that the PB power law with an exponent $n = -1.8$ describes the experimental data well. This indicates that the state of graphite has a very little effect on the electrical energy conduction of the copper–graphite composite. The electrical conductivity of the composite is mainly determined by the content of copper.

3.3.3 Mechanical Behavior of the Composites. Figure 10 shows the effect of graphite content on the compression strength of Cu$_2$O-Gr composites and Cu-Gr composites. The compression strength of both composites decreases with the increasing graphite content, and the strength of Cu$_2$O-Gr composites is about 50-100 MPa higher than that of Cu-Gr composites at any given graphite content. The Cu$_2$O-30Gr composite has a compression strength of up to 268 MPa. The high compression strength of Cu$_2$O-Gr composite should be attributed to much more smaller-sized and homogeneously dispersive graphite phase in the continuous copper phase resulted from the redox reaction at the interface between cuprous oxide and graphite.

According to the above experimental results, the improved bonding between copper and graphite in Cu$_2$O-Gr composite is
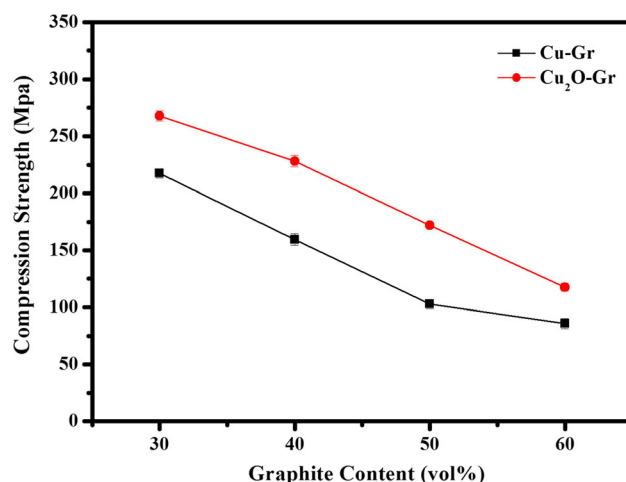
Table 3 Electrical resistivity of the composites

Composite	Content of graphite, vol.%	Electrical resistivity, μΩ m
Cu$_2$O-30Gr	30	0.0328 ± 0.006
Cu-30Gr	30	0.0327 ± 0.004
Cu$_2$O-40Gr	40	0.0420 ± 0.005
Cu-40Gr	40	0.0417 ± 0.006
Cu$_2$O-50Gr	50	0.0603 ± 0.008
Cu-50Gr	50	0.0604 ± 0.006
Cu$_2$O-60Gr	60	0.0947 ± 0.007
Cu-60Gr	60	0.0952 ± 0.009
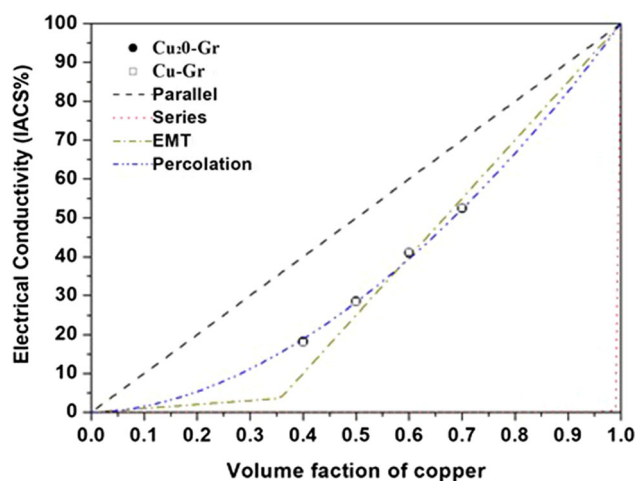
Fig. 9 Comparison between the experimental data and prediction values by different models

Fig. 10 Variation in compression strength with graphite content of Cu-Gr and Cu$_2$O-Gr composites

obvious. In Cu-Gr composites, graphite particles occupy the grain boundaries; however, the small pores cannot be filled by micron-sized particles (Ref 20). In the case of the Cu$_2$O-Gr composite powder mixtures, the cuprous oxide particles could react with the adjacent graphite particles, leading to the decrease in the particle size and the increase in the surface roughness of graphite particles under the pressure and high temperature during hot pressing sintering. During hot pressing sintering, the smaller-sized cuprous oxide particles could be embedded in larger-sized graphite particles. The bonding between particles becomes much stronger, leading to the strong interface between matrix and graphite and less porosity in the sintered samples.

Figure 11 shows the SEM images of the fracture surfaces of Cu-50Gr and Cu$_2$O-50Gr composites. The fracture surface of the Cu-50Gr composite is smoother than that of the Cu$_2$O-50Gr composite; however, the distribution of graphite phase on the facture surface in Cu-50Gr composite is uneven. The lamellar particles shown on the fracture surfaces of Cu-50Gr composite are the pulled-out graphite particles, which reveal that the composite has undergone a brittle fracture. For Cu$_2$O-50Gr composite, the distribution of graphite on the facture surface is much uniform. The dimple appears in the fractured sample, indicating that the copper in Cu$_2$O-50Gr composite undergoes a ductile deformation in some extent. Therefore, it can also be proved that the in situ reaction between cuprous oxide and graphite increases the bonding strength between copper and

graphite, leading to uniform deformation and large strain of Cu$_2$O-Gr composites during compression.

In the compression tests, it was found that all samples fractured at an inclined angle of about 45°, suggesting that the incorporation of graphite into Cu-matrix probably overstrains the lattice of copper atoms, leading to fracture the samples before attaining its potential strength and brittle failure (Ref 25). The larger-sized and agglomerated graphite particles in Cu-Gr composites tend to disintegrate from the center under pressure, leading to pore formation and brittle fracturing (Ref 8, 26), whereas the smaller-sized and finer dispersion of graphite particles in the matrix of Cu$_2$O-Gr composites could prevent the production and the propagation of the microcracks in the composites (Ref 11, 27). Samal et al. (Ref 11) prepared copper–graphite metal matrix composites through milling and sintering techniques and reported that the increase in the compressive strength is due to introduction of large amount of defects, improved dispersion during milling and strain hardening effect. Seah et al. (Ref 27) fabricated cast ZA-27/graphite composite and reported that the increase in compression strength is due to graphite particle acting as barriers to the dislocation in the microstructure. So the large amount of smaller-sized and much more homogeneously distributed graphite particles in the Cu$_2$O-Gr composites could also help to prevent the production and the propagation of the microcracks in the copper phase. Besides, the improved interface bonding between Cu and graphite particles in Cu$_2$O-Gr composites due to the in situ reaction at the interface is the other main strengthening
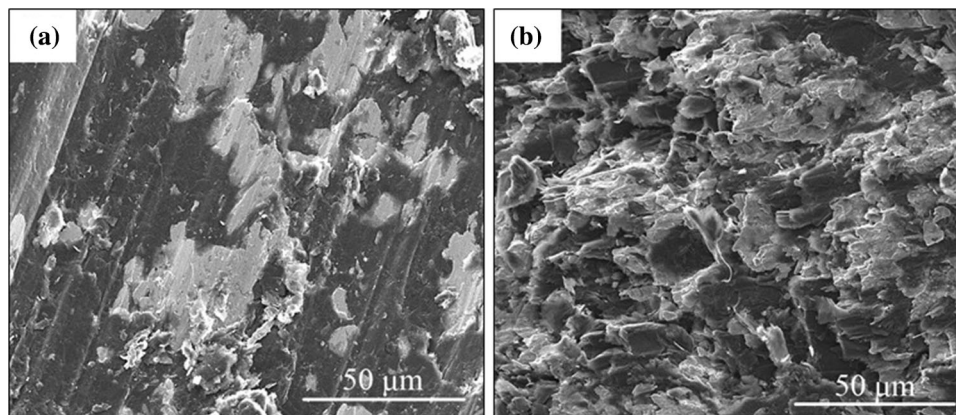
Fig. 11 SEM micrographs of the fracture surface of (a) Cu-50Gr and (b) Cu_2O-50Gr
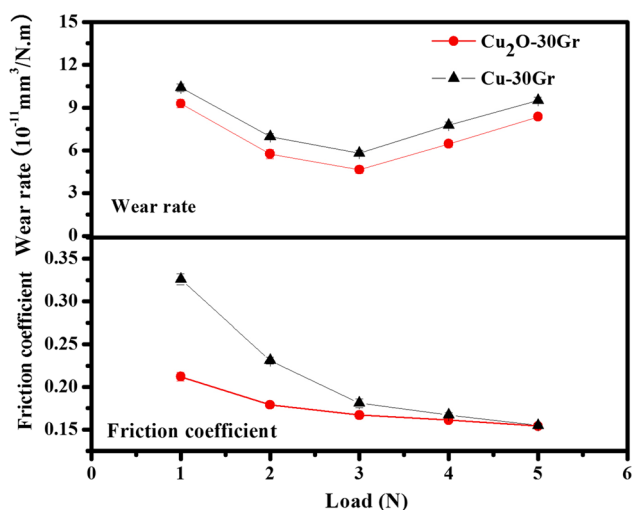
Fig. 12 Friction coefficient and wear rate of Cu-30Gr and Cu_2O-30Gr composite under different loads

mechanism (Ref 8). The copper and graphite in the Cu-Gr composites are weakly bonded by mechanical bonding, leading to the presence of gaps and high porosity content, whereas for the Cu_2O-Gr composites, the particle–particle contact is more closely bonded, leading to a relatively high compression strength of the Cu_2O-Gr composites. Recently, Kumar et al. (Ref 28) reported that the graphite-reinforced copper composite produced by milling and powder metallurgy had a good mechanical properties; however, the compression strength for copper composite with 15 wt.% (about 40 vol.%) graphite was about 110 MPa, which was less than half of the Cu_2O-40Gr composites in this study (about 230 MPa). This could be also attributed to the elimination of pores and strong bonding between copper matrix and graphite in Cu_2O-Gr composites. The Cu_2O-60Gr composite still has a compression strength up to 120 MPa; therefore, it would be expected that the ''In situ'' method can be an idea technique to produce copper–graphite composite with the high content of graphites.

Figure 12 shows the friction coefficient and wear rate of Cu-30Gr and Cu_2O-30Gr composite under different loads. The friction coefficient of both samples decreases with the load. At the relative low load, the graphite in the matrix cannot form the continuous lubrication film due to the small wear loss (Ref 15).

Large sliding load increases the amount of lubricant particles that squeezed out from the subsurface of the matrix, leading to the formation of continuous lubrication film and the decrease of friction coefficient (Ref 16, 29). Especially, the effect of load on the frication coefficient becomes less prominent as the load exceeds 3 N. The friction coefficient of Cu_2O-30Gr composite is less than that of Cu-30Gr composite at the low sliding load, suggestion that the continuous lubrication film in Cu_2O-30Gr composite is much easy to form. Rahjynar et al. (Ref 20) reported that the small size and uniform distribution of lubricant particle in the self-lubrication composite would promote the formation of continuous lubrication film on the contacting surface between the composite and disk. According to the SEM images shown in Fig. 6, compared with Cu-30Gr composite, the graphite particles in Cu_2O-30Gr composite are smaller and their distribution is more uniform, leading to better lubrication performance at the relative low load. The friction coefficient of both samples at a load of 5 N is close to each other, suggesting the formation of continuous lubrication films in both samples. The wear rates in both samples decrease first and then increase. At the relative low load, the increase in lubrication film decreases the wear rate of composite (Ref 29). A higher load could cause a greater extent of plastic deformation and lead to more severe wear of the composites, resulting in the increase in wear rate (Ref 15). However, the wear rate of Cu_2O-30Gr composite is less than that of Cu-30Gr composite at any given load, which could be attributed to the higher hardness and strength of Cu_2O-30Gr composite.

4. Conclusion

1. The copper–graphite metal matrix composites were satisfactorily produced by in situ reaction ($2Cu_2O(s) + C(graphite) \rightarrow 4Cu(s) + CO_2(g)\uparrow$) using cuprous oxide and graphite. Thus, during the sintering process (redox reaction) it is proved that it occurs at the interface of the Cu_2O-Gr composite powder mixtures and, consequently, leads to improve the hardness and compression strength values of the Cu_2O-Gr composites.
2. The values of electrical resistivity of Cu_2O-Gr composite and Cu-Gr composite are close to each other at any given

graphite contents. The variation in the electrical conductivity of copper–graphite composite with graphite content obeys to the percolation theory.

3. The compression strength of Cu_2O-Gr composite is 50-100 MPa higher than that of Cu-Gr composite at any given graphite contents due to the improved interface bonding and uniformly distributed fine graphite particles in the matrix.

References

1. Q. Liu, X.-B. He, S.-B. Ren, C. Zhang, L. Ting-Ting, and X.-H. Qu, Thermophysical Properties and Microstructure of Graphite Flake/Copper Composites Processed by Electroless Copper Coating, *J. Alloys Compd.*, 2014, **587**, p 255–259
2. S.-J. Guo, Q.-S. Yang, X.Q. He, and K.M. Liew, Modeling of Interface Cracking in Copper–Graphite Composites by MD and CFE Method, *Compos. B Eng.*, 2014, **58**, p 586–592
3. J. Chen, S. Ren, X. He, and X. Qu, Properties and Microstructure of Nickel-Coated Graphite Flakes/Copper Composites Fabricated by Spark Plasma Sintering, *Carbon*, 2017, **121**, p 25–34
4. W. Yang, L. Zhou, K. Peng, J. Zhu, and L. Wan, Effect of Tungsten Addition on Thermal Conductivity of Graphite/Copper Composites, *Compos. B Eng.*, 2013, **55**, p 1–4
5. G.F. Bocchini, The Influence of Porosity on the Characteristics of Sintered Materials, *Rev. Powder Metall. Phys. Ceram.*, 1985, **2**, p 313–359
6. J. Kováčik, Š. Emmer, J. Bielek, and L. Keleši, Effect of Composition on Friction Coefficient of Cu–Graphite Composites, *Wear*, 2008, **265**, p 417–421
7. F. Akhlaghi and A. Zare-Bidaki, Influence of Graphite Content on the Dry Sliding and Oil Impregnated Sliding Wear Behavior of Al 2024–Graphite Composites Produced by In Situ Powder Metallurgy Method, *Wear*, 2009, **266**, p 37–45
8. S.F. Moustafa, S.A. El-Badry, A.M. Sanad, and B. Kieback, Friction and Wear of Copper–Graphite Composites Made with Cu-Coated and Uncoated Graphite Powders, *Wear*, 2002, **253**, p 699–710
9. S. Saraswat, S. Tewari, and P.N. Rai, Impact of Brass and Electroplating Industry Effluent on Some Physico-chemical and Biological Properties of Soil, *J. Sci. Ind. Res.*, 2007, **66**, p 957–962
10. B. Liu, D. Zhang, X. Li, Z. He, X. Guo, and Z. Liu, Effect of Graphite Flakes Particle Sizes on the Microstructure and Properties of Graphite Flakes/Copper Composites, *J. Alloys Compd.*, 2018, **766**, p 382–390
11. C.P. Samal, J.S. Parihar, and D. Chaira, The Effect of Milling and Sintering Techniques on Mechanical Properties of Cu–Graphite Metal Matrix Composite Prepared by Powder Metallurgy Route, *J. Alloys Compd.*, 2013, **569**, p 95–101
12. Z. Tao, Q. Guo, X. Gao, and L. Liu, The Wettability and Interface Thermal Resistance of Copper/Graphite System with an Addition of Chromium, *Mater. Chem. Phys.*, 2011, **128**, p 228–232
13. S.M. Devincent and G.M. Michal, Improvement of Thermal and Mechanical Properties of Graphite/Copper Composites Through Interfacial Modification, *J. Mater. Eng. Perform.*, 1993, **2**, p 323–331
14. S. Ren, J. Chen, X. He, and X. Qu, Effect of Matrix-Alloying-Element Chromium on the Microstructure and Properties of Graphite Flakes/Copper Composites Fabricated by Hot Pressing Sintering, *Carbon*, 2018, **127**, p 412–423
15. H. Cao, Z. Qian, L. Zhang, J. Xiao, and K. Zhou, Tribological Behavior of Cu Matrix Composites Containing Graphite and Tungsten Disulfide, *Tribol. Trans.*, 2014, **57**, p 1037–1043
16. S. Huang, Y. Feng, H. Liu, K. Ding, and G. Qian, Electrical Sliding Friction and Wear Properties of Cu–MoS_2–Graphite–WS_2 Nanotubes Composites in Air and Vacuum Conditions, *Mater. Sci. Eng. A*, 2013, **560**, p 685–692
17. J. Li, L. Zhang, J. Xiao, and K. Zhou, Sliding Wear Behavior of Copper-Based Composites Reinforced with Graphene Nanosheets and Graphite, *Trans. Nonferr. Met. Soc. China*, 2015, **25**, p 3354–3362
18. C.B. Lin, Z.C. Chang, Y.H. Tung, and Y.Y. Ko, Manufacturing and Tribological Properties of Copper Matrix/Carbon Nanotubes Composites, *Wear*, 2011, **270**, p 382–394
19. Z.Y. Chen, *Chermodynamics of Refractories*, Metallurgical Industry Press, Beijing, 2005, p 648–649
20. K. Rajkumar and S. Aravindan, Tribological Behavior of Microwave Processed Copper–Nanographite Composites, *Tribol. Int.*, 2013, **57**, p 282–296
21. H. Kato, M. Takama, Y. Iwai, K. Washida, and Y. Sasaki, Wear and Mechanical Properties of Sintered Copper–Tin Composites Containing Graphite or Molybdenum Disulfide, *Wear*, 2003, **255**, p 573–578
22. N. Maraşlı, E. Çadirli, H. Kaya, U. Böyük, S. Aksöz, and Y. Ocak, Dependency of the Thermal and Electrical Conductivity on the Temperature and Composition of Cu in the Al Based Al–Cu Alloys, *Exper. Therm. Fluid Sci.*, 2010, **34**, p 1507–1516
23. The Electrical Landauer, Resistance of Binary Metallic Mixtures, *J. Appl. Phys.*, 1952, **23**, p 779–784
24. M.F. Ashby, T. Evans, N.A. Fleck, J.W. Hutchinson, H.N.G. Wadley, and L.J. Gibson, *Metal Foams: A Design Guide*, Elsevier, Amsterdam, 2000
25. I. Kudish, A New Statistical Model of Contact Fatigue, *Tribol. Trans.*, 2000, **43**, p 711–721
26. H. Kurita, T. Miyazaki, A. Kawasaki, Y. Lu, and J.-F. Silvain, Interfacial Microstructure of Graphite Flake Reinforced Aluminum Matrix Composites Fabricated Via Hot Pressing, *Compos. Part A: Appl. Sci. Manuf.*, 2015, **73**, p 125–131
27. K.H.W. Seah, S.C. Sharma, and B.M. Girish, Mechanical Properties of Cast ZA-27/Graphite Particulate Composites, *Mater. Des.*, 1995, **16**, p 271–275
28. J. Kumar and S. Mondal, Microstructure and Properties of Graphite-Reinforced Copper Matrix Composites, *J. Braz. Soc. Mech. Sci. Eng.*, 2018, **40**, p 196
29. N.K. Myshkin and V.V. Konchits, Friction and Wear of Metal-Composite Electrical Contacts, *Wear*, 1992, **158**, p 119–140

Publisher's Note Springer Nature remains neutral with regard to jurisdictional claims in published maps and institutional affiliations.